

# Free-energy landscape of polymer–crystal polymorphism

Chan Liu,<sup>1</sup> Jan Gerit Brandenburg,<sup>2,3</sup> Omar Valsson,<sup>1</sup> Kurt Kremer,<sup>1</sup> and Tristan Bereau<sup>1,4, a)</sup>

<sup>1)</sup>Max Planck Institute for Polymer Research, 55128 Mainz, Germany

<sup>2)</sup>Interdisciplinary Center for Scientific Computing, University of Heidelberg, 69120 Heidelberg, Germany

<sup>3)</sup>Digital Organization, Merck KGaA, 64293 Darmstadt, Germany

<sup>4)</sup>Van 't Hoff Institute for Molecular Sciences and Informatics Institute, University of Amsterdam, Amsterdam 1098 XH, The Netherlands

(Dated: 24 July 2020)

Polymorphism rationalizes how processing can control the final structure of a material. The rugged free-energy landscape and exceedingly slow kinetics in the solid state have so far hampered computational investigations. We report for the first time the free-energy landscape of a polymorphic crystalline polymer, syndiotactic polystyrene. Coarse-grained metadynamics simulations allow us to efficiently sample the landscape at large. The free-energy difference between the two main polymorphs,  $\alpha$  and  $\beta$ , is further investigated by quantum-chemical calculations. The two methods are in line with experimental observations: they predict  $\beta$  as the more stable polymorph at standard conditions. Critically, the free-energy landscape suggests how the  $\alpha$  polymorph may lead to experimentally observed kinetic traps. The combination of multiscale modeling, enhanced sampling, and quantum-chemical calculations offers an appealing strategy to uncover complex free-energy landscapes with polymorphic behavior.

## I. INTRODUCTION

The complex interplay of molecular interactions can lead to a material exhibiting multiple distinct forms in its solid state.<sup>1</sup> This polymorphism often results in widely different materials properties, making the study of polymorphism both essential for quality control in manufacture, but also a fascinating structure–property problem. Beyond structure and property, the intermediate processing of the material has a key impact on the resulting polymorph. Fundamentally this stems from two ingredients: (i) the underlying free-energy landscape is sufficiently rugged to display several low-lying metastable states; and (ii) exceedingly slow kinetics exhibited in the solid phase, preventing a full/ergodic kinetic relaxation.

The screening of polymorphs has traditionally exclusively been performed experimentally, in spite of the significant costs involved. Computational methods hold the promise of predicting polymorphic stability before going to the laboratory. In the context of molecular crystals, especially targeted at pharmaceuticals and porous (organic) cages, a considerable body of work has recently emerged.<sup>2–13</sup> The modeling of polymorphism holds two challenges: sampling and modeling accuracy. The free-energy landscape exhibits an overwhelming number of configurations, of which only an infinitesimal fraction competes in terms of low-lying states. Furthermore, correctly ranking the relative free energies of each conformer requires computational methods that are accurate enough (of the order of thermal energy,  $k_B T$ ) to reproduce the underlying interactions. Many methods exist to tackle these two challenges, out of which we mention the use of an appropriately-tuned force-field based method

for the sampling and electronic-structure methods (e.g., density functional theory) for the energetic characterization.<sup>14–16</sup>

Here, we focus on polymers, which not only embody countless industrial applications, but also for which we critically lack a detailed picture of its free-energy landscape. Evidently, the increased number of atoms per molecule involved will lead to higher structural correlations, significantly larger barriers, and much longer timescales compared to molecular crystals of small molecules. While many semicrystalline polymers possess only a single type of unit cell, there are exceptions: syndiotactic polystyrene (sPS) for instance is well-known for its complex crystal polymorphism.

In this work, we aim at unraveling the underlying free-energy landscape of sPS, to better understand the body of experimental evidence gathered around its polymorphs. We focus on the thermally-induced processing aspect—the  $\alpha$  and  $\beta$  polymorphs, shown in Fig. 1.<sup>18–23</sup> They share the same intrachain conformations, but with different interchain-packing structures. The  $\alpha$  and  $\beta$  forms of sPS are further classified into limiting disordered forms,  $\alpha'$  and  $\beta'$ , and limiting ordered forms,  $\alpha''$  and  $\beta''$ .<sup>18,20,22,24</sup> The processing conditions impact the forms experimentally observed.<sup>22,24</sup> Fig. 1 displays the limiting ordered forms.

Experimental evidence has pointed out the strong impact of the processing conditions: starting material, initial temperature, and cooling rate.<sup>18,22,24–28</sup> They hint at a highly complex free-energy landscape. The relative stability between the  $\alpha$  and  $\beta$  polymorphs is noteworthy: (i) Starting from a high initial temperature, a fast (slow) cooling will lead to the  $\alpha$  ( $\beta$ ) forms; (ii) Under identical slow cooling rate, melt crystallization starting under 230°C and above 260°C will yield the  $\alpha$  and  $\beta$  polymorphs, respectively, while intermediate temperatures generate mixtures thereof. These results suggest

<sup>a)</sup>Electronic mail: t.bereau@uva.nl

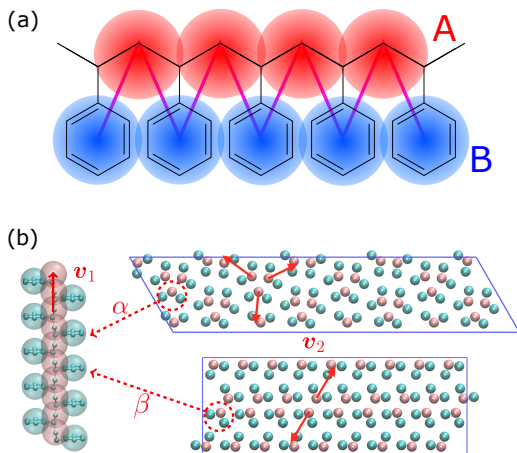


FIG. 1. (a) Molecular structure of polystyrene and CG-mapping scheme of the Fritz model.<sup>17</sup> (b) Left: Longitudinal view of an all-trans chain conformation; Right: transverse section of the experimentally-resolved  $\alpha$  and  $\beta$  forms. In the transverse sections, each polymer chain is represented by three CG beads (highlighted in red dashed circles). The red solid lines represent cross-sectional vectors pointing from the backbone to the bisector of its two closest side chains.

that given sufficient mobility thanks to a high initial temperature and a slow enough cooling rate, the preferred packing structure corresponds to the  $\beta$  form. In case of stiffened chains and/or reduced molecular mobility, the  $\alpha$  polymorph is preferred. These glimpses at the structural properties of sPS indicate that crystallization to the  $\alpha$  form results from a kinetically-controlled process, while  $\beta$  would be the thermodynamically stable form. Our understanding thereby falls short in several ways: how the free-energy landscape translates into the apparent differences between the two forms, but also a more mechanistic insight as to the origin of these effects.

While computational studies of polymer crystal polymorphs remain to date extremely limited, we note the work of Tamai and co-workers on nanoporous cavity structures in the  $\alpha$  and  $\beta$  forms,<sup>29</sup> the diffusion of gases,<sup>30,31</sup> the orientational motion of guest solvents,<sup>32,33</sup> and the adsorption of small molecules.<sup>34–36</sup> These studies helped understand structural features of some of these forms. Unfortunately the atomistic resolution involved strongly limit the timescale that can be reached with the simulations—on the order of nanoseconds. This prevents both the observation of self assembly, but also polymorph interconversion, thereby hindering access to the free-energy landscape.

To address the time-scale issue, we turn to coarse-grained (CG) modeling. By lumping several atoms into one larger superparticle or bead, CG models can sample significantly faster, while offering a systematic connection to the reference chemistry.<sup>37</sup> Some of us recently applied a structure-based CG model aimed at reproducing certain thermodynamic aspects of sPS.<sup>17</sup> Despite a parametrization and validation performed exclusively in

the melt, we found remarkable transferability to the crystalline phase: not only does the CG model stabilize the  $\alpha$  and  $\beta$  polymorphs, the melting temperatures of the two phases were found to be in excellent agreement.<sup>38</sup> Our study aimed at an exploration of the self-assembly mechanisms of sPS, using a temperature-based enhanced-sampling molecular dynamics (MD) techniques—parallel tempering. In the present work, we instead turn to methods based on collective variables (CVs), specifically metadynamics.<sup>39,40</sup> We will show that an appropriate choice of CVs can lead to convergence of the simulations, and offer us access to a great diversity of structural forms. We present for the first time the free-energy landscape of polymorphism of a polymer crystal.

We further challenge the calculations of the free-energy difference between  $\alpha$  and  $\beta$  polymorph stability by means of quantum-chemical calculation at the density functional theory (DFT) level. The results show excellent agreement with the CG simulations given the change in resolution. Critically, we find in both cases the preferential stabilization of the  $\beta$  phase—in line with experiments.

## II. RESULTS AND DISCUSSION

### A. Metadynamics

In the Methods we present collective variables (CVs) that are capable of distinguishing five different phases of sPS (Sec. IV B). A significant distinction between these phases is essential to also enable the discovery of other intermediate phases. A further requirement is the absence of hidden barriers that would hinder dynamics along the CVs.<sup>39</sup> To alleviate possible artifacts due to an inappropriate choice of CVs, we test several of them and later reweight all simulations to the same CV space. This further allows us to empirically check the convergence of our simulations.

We focus on a two-dimensional CV exploration, as a balance between exploration and convergence: a three-dimensional CV-space exploration can require excessive memory and presents challenges to converge due to the curse of dimensionality. We note that extensions of the method, such as bias-exchange and parallel-bias metadynamics, can help along these lines.<sup>41–44</sup> We herein present four combinations of CVs referenced in Tab. S1: (i)  $\Delta\mathcal{S}$  &  $\mathcal{S}_1$ ; (ii)  $\Delta\mathcal{S}$  &  $\mathcal{S}_2$ ; (iii)  $\Delta\mathcal{S}$  &  $\mathcal{S}_3$ ; (iv)  $\Delta\mathcal{S}$  &  $P_2(\mathbf{v}_2)$ .

Fig. S5 shows a metadynamics simulation at  $T = 400$  K driven by the combination of CVs  $\Delta\mathcal{S}$  &  $P_2(\mathbf{v}_2)$  using two walkers. The walkers were initiated from the two crystalline phases  $\alpha$  and  $\beta$ . The simulations are able to transition many times between the main polymorphs, starting at around 20 ns (Fig. S5a). The results highlight that the ability of the CVs to distinguish  $\alpha$  from  $\beta$  help ensure large conformational transitions (Fig. S2). We note however the absence of conformations in the amorphous phase, due both to our sampling below the transition temperature (roughly 450 K) and our protocol’s restrain-

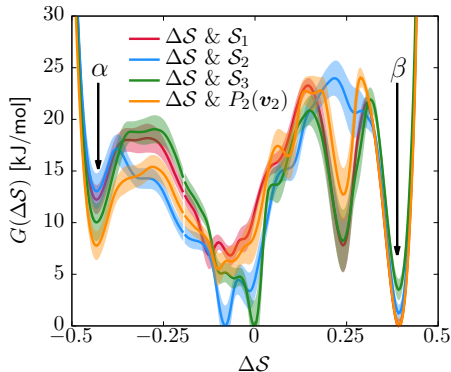


FIG. 2. Convergence of the free-energy calculations. Comparison of four metadynamics simulations at  $T = 400$  K with different CVs (see labels) projected on  $\Delta S$ .

ing box range and chain direction (see Sec. IV C).

## B. Polymorphic stability

Having established that our combinations of CVs enables a satisfactory transition between major polymorphs, we turn to the question of convergence. To assess convergence, we run metadynamics in the CV space of our four combinations, and marginalize the free-energy landscape to only display their common CV: the SMAC difference  $\Delta S$ . Fig. 2 compares the free-energy surface as a function of the CV,  $G(\Delta S)$ . We have marked the  $\alpha$  and  $\beta$  polymorphs according to values of the CV from unbiased MD simulations (see SI). All four curves agree within roughly 5 kJ/mol across the range of  $\Delta S$  values, despite their sampling along different complementary CV. Convergence as a function of simulation time is further displayed in Fig. 3a, which focuses on the free-energy difference between the  $\alpha$  and  $\beta$  polymorphs,  $G_\alpha - G_\beta$ . We find that all curves converge after roughly 1 to 2  $\mu$ s. We do see variations between simulations reminiscent of the spread in panel (a). Given the remarkable complexity of probing the free-energy landscape of polymer crystals, we consider this level of agreement encouraging indicators of the level of convergence of our simulations.

Metadynamics simulations on different system sizes lead to similar free-energy profiles (see Fig. S6), whether changing the number of chains in the box or the number of monomers per chain. We rationalize the lack of system-size dependence in two ways: (i) The lack of dependence in the number of chains can be explained by the collective nature of the transitions, where the box is so small that all chains transition to a new phase at once; and (ii) The free-energy barriers do not scale with the number of monomers, because the transitions are orthogonal to the chain director, as indicated by the order parameters  $P_2(\mathbf{v}_1)$  and  $P_2(\mathbf{v}_2)$  (see Fig. S2).

Having identified the two polymorphs as local min-

ima with a rationalization of kinetic routes in between them, we try to further establish their relative thermodynamic stability. For this, we use the structures identified in the dynamics and employ quantum mechanical methods for local structure relaxations and prediction of their temperature dependent free energy (see section IV D). In contrast to the molecular dynamics simulations, our DFT results do not describe anharmonicities of the energy surface, potentially neglecting some thermal effects. On the other hand, the described interactions are at a quantum mechanical level, physically more sound, and thus expected to be more accurate compared to the classical potentials used in our molecular dynamics. We show in Fig. 3b the quantum-mechanical energy difference between the two polymorphic forms. In a static picture at 0 K, sPS  $\beta$  is predicted to be more stable by 4 kJ/mol. Heating to 400 K, the enthalpy difference increases by 1 kJ/mol, while the free energy difference decreases by 3 kJ/mol. At elevated temperatures of about 500 K, form  $\alpha$  is predicted to be more stable, which is, however, not experimentally observable due to the amorphous phase. The stability difference at room temperature is in excellent agreement with the estimations from our dynamics simulations indicating a stabilization of  $\beta$  by 5-10 kJ/mol. The smaller stability difference predicted by DFT is in line with our experience from molecular crystals, where higher quality interaction energy models typically lead to smaller energy gaps between polymorphs.<sup>14</sup> The overall analysis matches the experimental expectation that form  $\alpha$  crystallizes by rapid cooling from elevated temperatures, while  $\beta$  forms in slow cooling experiments.<sup>45</sup>

The analysis reported in Fig. 3 shows that the  $\beta$  form is systematically better stabilized than the competing  $\alpha$  form. The 1D landscape clearly separates  $\alpha$  from  $\beta$  at the left and right sides of the range, respectively. These are separated by both  $\alpha/\beta$  mixtures and the amorphous phases at around  $\Delta S \approx 0$ . Interestingly, we observe a significantly lower free-energy barrier upon going from the amorphous phase to the pure  $\alpha$  polymorph, than the  $\beta$  polymorph: while the former is between 10 and 15 kJ/mol high, the other is upwards of 20 kJ/mol. The  $\beta$  form is more stable across the CV space, but the  $\alpha$  form is easier to *reach* from the mixture and amorphous phases—a kinetic effect. This can help rationalize the kinetic-trap behavior of the  $\alpha$  form found experimentally.<sup>45</sup> Some of us had previously identified an overpopulation of the  $\alpha$  form when probed in simulation box geometries concomitant to the  $\alpha$  unit cell, suggesting a templating mechanism.<sup>38</sup>

## C. Free-energy landscape of sPS

As an extension to Fig. 2, Fig. 4 shows a representation of the free-energy landscape for the CV combination  $\Delta S$  &  $S_1$ . Stability is color coded from blue to red. We observe a large diversity of phases with distinct structural

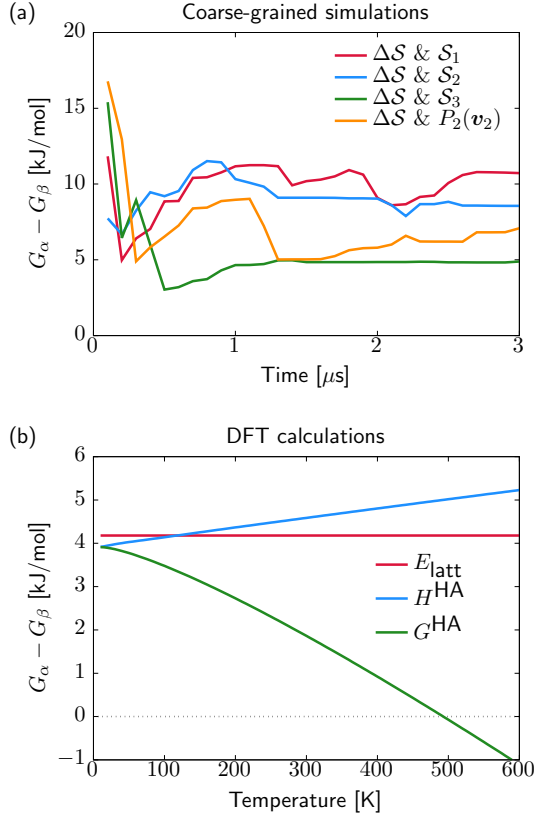


FIG. 3. Free-energy difference between  $\alpha$  and  $\beta$  forms. (a) The CG simulations show the time evolution of  $G_\alpha - G_\beta$  from the different Metadynamics simulations. (b) The DFT-based stability differences at standard pressure and as a function of temperature, including lattice energy  $E_{\text{latt}}$ , enthalpy  $H^{\text{HA}}$ , and free energy  $G^{\text{HA}}$ .

features. Notably, we find many more structures than our previous study based on parallel tempering.<sup>38</sup>

We first analyze structures similar to the  $\alpha$  polymorph. Of particular interest are symmetries around triplets of chains that form the fundamental symmetric unit of  $\alpha$  structures (see Fig. 1b). As compared to our previous work that used parallel tempering, we observe a broader variety of relative orientations between chain triplets: Small but noticeable variations can be found among the  $\alpha$ -type structures on the landscape. The differentiation between  $\alpha'$  and  $\alpha''$  is made more difficult by imposing 12 chains in our simulation box, while the unit cell of  $\alpha$  contains only 9 chains.<sup>20</sup> We emphasize the difference between apparently distinct forms stabilized in our simulations:  $\alpha'$ ,  $\alpha'_{\text{defect}}$  and  $\alpha''_{\text{like}}$ , shown in Fig. 4. All triplets of chains, represented by groups of tan-colored beads, exhibit virtually identical orientations in  $\alpha'$  and little variation in  $\alpha'_{\text{defect}}$ : the angles between side-chain vectors are almost strictly at  $120^\circ$ , leading to  $\Delta S \approx -0.4$ .  $\alpha''_{\text{like}}$ , on the other hand, displays two different triplet orientations, analogous to the experimentally resolved  $\alpha''$ . The angles between side-chain vectors does not always corre-

spond to  $120^\circ$ , leading to  $\Delta S \approx -0.2$ , located near the mixture phases. Our simulations do not stabilize the  $\alpha''$  polymorph, which may be due to the number of chains incongruent with the unit cell, or possibly limitations in the CG force field in reproducing fine steric features.<sup>17,38</sup>

In line with our previous study, we find an alternate form to the experimentally-resolved<sup>22,24</sup> limiting disordered  $\beta'$  and limiting ordered  $\beta''$  polymorphs as the most global minimum of sPS:  $\beta_{\text{sim}}$ , where we highlighted the difference in layering.<sup>38</sup> While the parallel tempering simulations led to neither experimental form, the metadynamics simulations successfully sampled them, albeit at too high free energy: the  $\beta'_{\text{exp}}$  and  $\beta''_{\text{exp}}$  forms sit at about 30 and 50 kJ/mol higher than the global minimum, respectively. We argued before that the simple description of the side-chain sterics likely had a detrimental effect on the stability of the  $\beta$  polymorphs. This effect was motivated by a discrepancy in the melting temperature from CG simulations, as compared to reference atomistic simulations: in excellent agreement for the  $\alpha$  form, but too-low stability for  $\beta$ . In the context of the present work, these structural artifacts likely give rise to shifts in the free-energy landscape shown in Fig. 4.

### III. CONCLUSION

In this paper, we study the free-energy landscape of syndiotactic polystyrene (sPS) using computational methods to get microscopic insight into polymorphic interconversion. The development of adequate collective variables (CVs) applied to metadynamics, together with the use of a remarkably transferable coarse-grained (CG) model allow us for the first time to cross the significant barriers between polymorphs in polymer crystals. Minute structural differences between polymorphs requires finely-tuned CVs to account for the small variations. Rather than relying on a single CV combination, running metadynamics on several such combinations and reweighing them helps us test for convergence of the simulations. We find excellent agreement between four such combinations, despite the significant barriers exerted by the system.

We rely on a combination of two different SMAC variables<sup>46</sup> to build a free-energy landscape. The  $\beta$  form clearly stands as the global minimum, even though we observe fine differences between the simulated and experimental layerings, arguably an artifact of the side-chain representation in the CG model. Encouragingly, we do observe the two experimental  $\beta'_{\text{exp}}$  and  $\beta''_{\text{exp}}$  structures in the metadynamics runs. The  $\alpha$  form is between 5 and 10 kJ/mol less stable than the global minimum. As a complementary approach, we used quantum mechanical models to compute the temperature dependent relative stability of the  $\alpha$  and  $\beta$  polymorphs. We predict the stability to be slightly smaller (1 kJ/mol), but can overall confirm the CG simulations.

Remarkably, we find a significantly lower free-energy



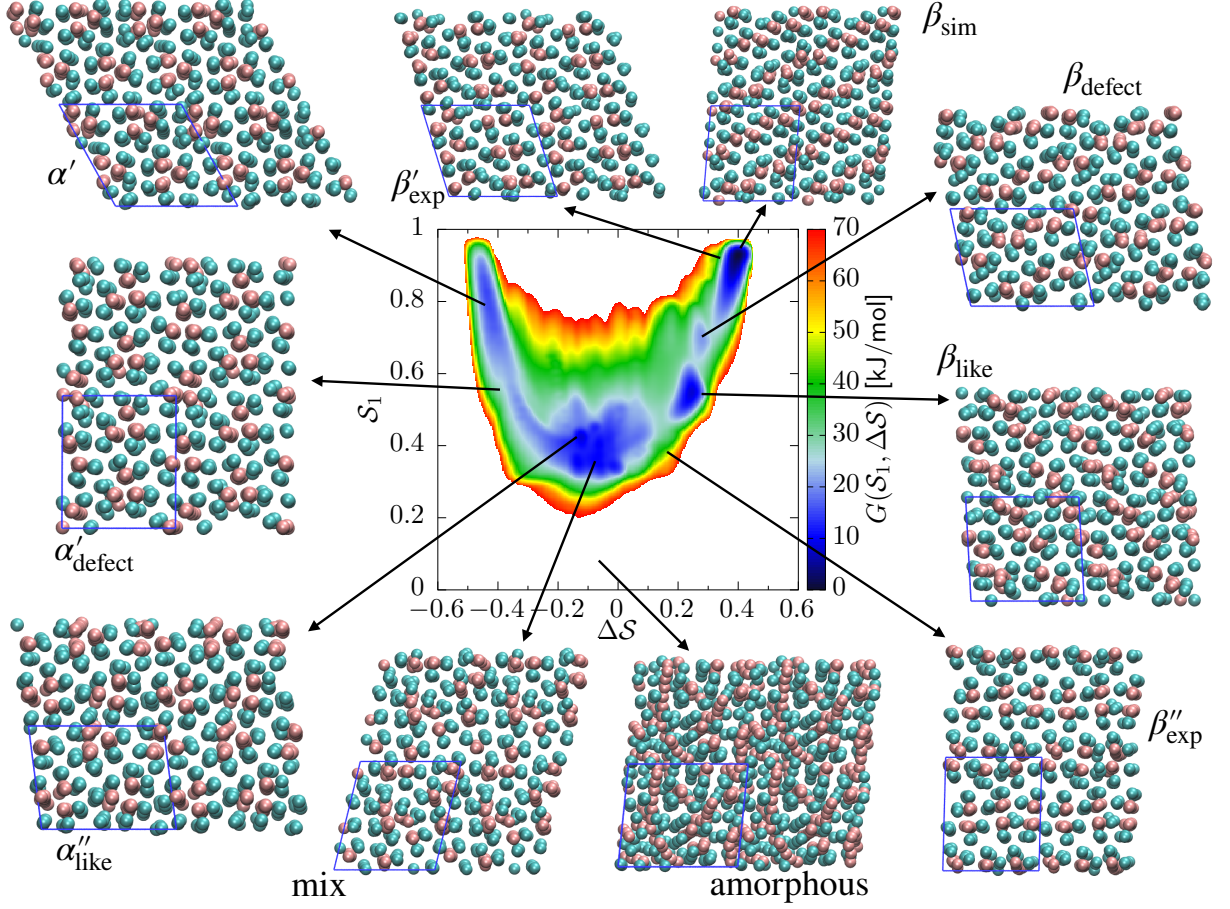


FIG. 4. Free-energy landscape of sPS sampled with metadynamics as a function of the CVs:  $G(S_1, \Delta S)$ . Various structures—representative of the simulations and/or the experiments—are displayed and identified on the surface.

*barrier* upon going from the amorphous phase to  $\alpha$  rather than  $\beta$ . This lowered activation could partially explain the  $\alpha$  polymorph’s tendency to be identified as a kinetic trap. It also complements our previous observation:  $\alpha$  is overstabilized in box geometries congruent with its unit cell, a templating mechanism of sorts. Differences in nucleation rates may further help drive the system in the direction of  $\alpha$ , although this is beyond the scope of this work.

Varying the system size will naturally affect the results: smaller simulation boxes are more likely to suffer from incompatibilities with different crystal units, resulting in artificially low stabilization. On the other hand, the significant free-energy barriers will become more challenging to cross as simulation boxes grow. The present study demonstrates that a multiscale approach can provide insight and complementary information to experiments on polymer–crystal polymorphism.

## IV. SIMULATION METHODS

### A. Coarse-grained simulations

We rely on a previously-developed coarse-grained (CG) model for syndiotactic polystyrene (sPS), referred hereafter as the Fritz model.<sup>17</sup> It maps each monomer onto two types of CG beads: “A” for the chain backbone and “B” for the phenyl ring (Fig. 1a). The model represents PS by a linear chain of alternating A and B CG beads, supplemented by sophisticated bonded potentials to ensure accurate structures, including the correct tacticity—enabling the crystallization of sPS. The bonded interactions were obtained by direct Boltzmann inversion of distributions obtained from atomistic simulations of single chains in vacuum. The nonbonded potentials are derived by the conditional reversible work (CRW) method:<sup>47,48</sup> constrained-dynamics runs with the all-atom model of two short chains in vacuum.

## B. Collective variables

Metadynamics acts on the selected CVs to drive the system and cross free-energy barriers. This puts an essential role on the choice of CVs, known to be extremely system and process dependent.<sup>39</sup> A large variety of CVs have been used, for instance, distances, angles, or dihedrals formed by atoms or groups of atoms,<sup>49</sup> coordination numbers,<sup>41,50,51</sup> and Steinhardt parameters.<sup>52–54</sup>

Crystallization is typically characterized by long-range order. For example, cluster symmetries are often probed via the Steinhardt parameter,  $Q_l$ ,<sup>55,56</sup> which represents the rotationally-invariant spherical harmonics of order  $l$ .  $Q_4$  and  $Q_6$ , in particular, have been studied in the context of Lennard-Jones particles,<sup>52</sup> ice,<sup>53</sup> and calcium carbonate nanoparticles.<sup>54</sup> To study polymorphism in sPS, however, we have found the Steinhardt parameter to inefficiently distinguish crystalline forms (see Fig. S3). We rationalize this by the lack of differentiation for transverse vectors (see Fig. 1b). This has led us to the development of CVs that are tailored to sPS.

Fig. 1b shows a longitudinal view of a chain conformation, as well as transverse sections of the two main polymorphs of interest: the experimentally-determined  $\alpha$  and  $\beta$  structures.<sup>24</sup> We herein propose two sets of vectors: one longitudinal vector,  $\mathbf{v}_1$ , and one transverse vector,  $\mathbf{v}_2$ .  $\mathbf{v}_1$  is oriented along the backbone, it is defined by the interparticle vector between two consecutive monomers (i.e., backbone beads). As for the transverse vector  $\mathbf{v}_2$ , for each monomer, it originates from the second backbone and point to the bisector of the two closest side chains. Fig. 1b indicates that typical angles for the  $\alpha$  and  $\beta$  polymorphs are roughly  $120^\circ$  and  $180^\circ$ , respectively. Note that here, to improve the efficiency of computation, the side-chain vector is an average over each whole molecule. Effectively this assumes a homogeneous configuration across the chain, in line with the system sizes considered here.

Because these two polymorphs consist of identical chain conformations, no differences can be extracted from *intrachain* statistics. Instead, differences between polymorphs are concentrated in the *interchain* configurations. As such, any CV that is to distinguish between polymorphs ought to focus on interchain geometries. By symmetry, the most noticeable differences occur along the transverse sections. These differences can be displayed more intuitively by the distribution of angles between neighboring transverse vectors  $\mathbf{v}_2$  (see Fig. S1), which is from unbiased MD simulations at 300 K. In the following, we will introduce two kinds of CVs which are functions of these transverse angles.

### 1. Legendre polynomial $P_2$

The second Legendre polynomial  $P_2$  probes the orientation between two vectors  $\mathbf{e}_i$  and  $\mathbf{e}_j$

$$P_2(\mathbf{e}) = \frac{3}{2}(\mathbf{e}_i \cdot \mathbf{e}_j)^2 - \frac{1}{2}. \quad (1)$$

$P_2$  is a natural candidate to describe orientational ordering and has been used to monitor the crystalline growth and/or state of polymer chains.<sup>57,58</sup> Some of us previously used  $P_2$  to monitor the melting transition of sPS.<sup>38</sup>

### 2. SMAC

Giberti et al.<sup>46</sup> recently introduced a CV to capture the inherent variety of crystal symmetries.<sup>59</sup> This CV, simply called SMAC in PLUMED, is formulated with the aim of accounting for both local density and the mutual orientation of molecules. In our case, it probes features of the angle distributions between transverse vectors, as shown in Fig. S1. It compares an input angle,  $\theta_{ij}$ , to a reference angle,  $\theta_n$ , via

$$K_n(\theta_{ij} - \theta_n) = e^{-((\theta_{ij} - \theta_n)^2 / 2\sigma_n^2)}. \quad (2)$$

This kernel smoothly interpolates from identical to distant angles leading to values from 1 to 0, respectively. SMAC relies on these kernels to probe one or multiple reference angles according to the phase of interest, supplemented by a smooth cutoff scheme

$$s_i = \frac{\left\{1 - \Psi \left[ \sum_{j \neq i} \sigma(r_{ij}) \right] \right\} \sum_{j \neq i} \sigma(r_{ij}) \sum_n K_n(\theta_{ij} - \theta_n)}{\sum_{j \neq i} \sigma(r_{ij})}. \quad (3)$$

Eq. 3 relies on the two switching functions  $\sigma(r) = \frac{1 - (r/r_\sigma)^6}{1 - (r/r_\sigma)^{12}}$  and  $\Psi(r) = \exp(-r/r_\Psi)$ , where  $r_\sigma$  and  $r_\Psi$  (see Tab. S1) provide a balance to keep the CV local, while incorporating enough numbers. The quantity is then averaged over all  $s_i$ :  $\mathcal{S} = \sum_{i=1}^N s_i / N$ .

Based on the angle distributions of Fig. S1, we construct a number of SMAC CVs using various sets of reference angles to optimally distinguish between sPS phases. Tab. S1 lists the set of CVs we used in this work. For instance, the main peaks for the  $\alpha$  and  $\beta$  phases led to the definition of SMAC CVs  $\mathcal{S}_\alpha$  and  $\mathcal{S}_\beta$ , centered at  $120^\circ$  and  $170^\circ$ , respectively. To emphasize both features at once, we constructed a CV based on their difference:  $\Delta\mathcal{S} = \mathcal{S}_\beta - \mathcal{S}_\alpha$ . This can be observed through a monitoring of the CV during unbiased MD simulations (Fig. S2c). Three additional SMAC CVs are presented in Tab. S1.

### C. Metadynamics

Well-tempered metadynamics simulations were performed at 400 K.<sup>40,60–65</sup> The bias deposition stride was set to be 0.5 ps, and the bias factor was 20. The Gaussian-bias width was set to 0.01 for  $\Delta S$ , and 0.05 otherwise. The initial Gaussian heights were all set to 3 kJ/mol. Each simulation consisted of multiple walkers.<sup>66</sup> In metadynamics, we refer to a biased run that explores the CV-space as a walker, while multiple walkers simultaneously explore and carve the same free-energy landscape. This method can significantly speed up the convergence of the simulations, as all walkers contribute to a single, combined free-energy landscape. In this work, 2 walkers were run in parallel and initialized from the  $\alpha$  and  $\beta$  forms, respectively. All simulations were performed using GROMACS 5.1.4<sup>67</sup> and PLUMED 2.4.<sup>68,69</sup> Simulations were carried out in the isothermal-isobaric ensemble at  $P = 1$  bar using the velocity-rescale thermostat<sup>70</sup> and the anisotropic Parrinello-Rahman barostat.<sup>71</sup> We ensured stable variations in the simulation box by restraining the range of allowed geometries ( $5 < a^2 < 9$ ;  $5 < b^2 < 9$ ;  $6 < c^2 < 8 \text{ nm}^2$ ). We also restrained the director of each chain to lie within  $30^\circ$  of the box's  $z$  component. This avoided significant collective rotations of the chains with respect to the simulation box, leading to alignments along the other coordinates. Such a scheme merely aims at enforcing all chains to loosely lie within an arbitrarily-chosen  $z$  axis. This helped avoid artifacts when calculating longitudinal and transverse vectors, especially at higher temperatures. More details can be found in the SI.

### D. Quantum-chemical methods

Quantum-chemical methods are used to simulate the relative thermodynamical stability of the two sPS polymorphs. The two polymorphic forms identified by the metadynamics simulations and experimentally characterized in the literature have been taken as starting points for local geometry optimization. Phonon modes are computed to confirm the stationary points as local minima and to give access to the temperature-dependent harmonic Gibbs free energy

$$G^{\text{HA}}(T, P) = E_{\text{latt}} + G_{\text{vib}}^{\text{HA}}(T) + PV. \quad (4)$$

Here,  $E_{\text{latt}}(V)$  is the zero-temperature internal energy of the crystal given per monomer unit—the lattice energy. The vibrational contributions are

$$G_{\text{vib}}^{\text{HA}}(T) = \sum_{\mathbf{k}, p} \frac{\hbar \omega_{\mathbf{k}, p}}{2} + k_{\text{B}} T \sum_{\mathbf{k}, p} \left[ \ln \left( 1 - e^{-\frac{\hbar \omega_{\mathbf{k}, p}}{k_{\text{B}} T}} \right) \right], \quad (5)$$

where the phonon frequencies  $\omega_{\mathbf{k}, p}$  correspond to a  $\mathbf{k}$ -point in first Brillouin zone and a phonon band index  $p$ .

The temperature-dependent harmonic enthalpy,  $H^{\text{HA}}$ , is described in the SI. The quantum chemical calculations are performed using density functional theory (DFT), which is the method of choice for many materials applications due to its favorable accuracy to computational cost ratio.<sup>72–75</sup> The DFT calculations are done with a screened exchange hybrid density functional, dubbed HSE-3c.<sup>76,77</sup> It combines accurate descriptions of geometries over a broad class of systems with an efficient treatment of non-local exchange and long-range London dispersion interaction.<sup>78,79</sup> For a general overview of dispersion corrections in the density functional framework and the treatment of molecular crystals see Refs. 80–82. The implementation of HSE-3c into the CRYSTAL17 program enables the fast computation of electronic structures and phonon modes using all point- and space-group symmetries.<sup>83,84</sup> Geometry optimizations are performed with tight convergence thresholds and in space groups  $P3_1$  ( $\alpha$ ) and  $Pnma$  ( $\beta$ ). The Brillouin zone has been sampled with a  $1 \times 1 \times 5$  and  $1 \times 5 \times 3$  grid for the  $\alpha$  and  $\beta$  polymorphs, respectively.  $\Gamma$ -point frequencies have been computed by sHF-3c,<sup>85,86</sup> above  $\Gamma$ -point frequencies are tested to be negligible at the DFTB3-D3 level,<sup>87–89</sup> which has been shown to be a reliable approach for organic solids.<sup>90</sup>

### V. ACKNOWLEDGMENT

We thank Christine Peter for insightful discussions, as well as Bingqing Cheng, Robinson Cortes-Huerto, and Hsiao-Ping Hsu for critical reading of the manuscript. CL was supported by the Max Planck Graduate Center. TB was partially supported by the Emmy Noether program of the Deutsche Forschungsgemeinschaft (DFG).

<sup>1</sup>Harry G Brittain et al. Polymorphism in pharmaceutical solids. *Drugs and the pharmaceutical sciences*, 95:183–226, 1999.

<sup>2</sup>Robert J Gdanitz. Ab initio prediction of molecular crystal structures. *Current Opinion in Solid State and Materials Science*, 3(4):414–418, 1998.

<sup>3</sup>Joel Bernstein and Joel M Bernstein. *Polymorphism in molecular crystals*, volume 14. Oxford University Press, 2002.

<sup>4</sup>Martin Jansen, Klaus Doll, and J. Christian Schön. Addressing chemical diversity by employing the energy landscape concept. *Acta Crystallographica Section A Foundations of Crystallography*, 66(5):518–534, August 2010.

<sup>5</sup>James T. A. Jones, Tom Hasell, Xiaofeng Wu, John Bacsa, Kim E. Jelfs, Marc Schmidtman, Samantha Y. Chong, Dave J. Adams, Abbie Trewin, Florian Schiffman, Furio Cora, Ben Slater, Alexander Steiner, Graeme M. Day, and Andrew I. Cooper. Modular and predictable assembly of porous organic molecular crystals. *Nature*, 474(7351):367–371, June 2011.

<sup>6</sup>Yuriy A. Abramov. Current computational approaches to support pharmaceutical solid form selection. *Organic Process Research & Development*, 17(3):472–485, December 2012.

<sup>7</sup>Edward O. Pyzer-Knapp, Hugh P. G. Thompson, Florian Schiffmann, Kim E. Jelfs, Samantha Y. Chong, Marc A. Little, Andrew I. Cooper, and Graeme M. Day. Predicted crystal energy landscapes of porous organic cages. *Chem. Sci.*, 5(6):2235–2245, 2014.

- <sup>8</sup>Aurora J. Cruz-Cabeza, Susan M. Reutzel-Edens, and Joel Bernstein. Facts and fictions about polymorphism. *Chemical Society Reviews*, 44(23):8619–8635, 2015.
- <sup>9</sup>M. A. Neumann, J. van de Streek, F. P. A. Fabbiani, P. Hidber, and O. Grassmann. Combined crystal structure prediction and high-pressure crystallization in rational pharmaceutical polymorph screening. *Nature Communications*, 6(1), July 2015.
- <sup>10</sup>Sarah L. Price and Susan M. Reutzel-Edens. The potential of computed crystal energy landscapes to aid solid-form development. *Drug Discovery Today*, 21(6):912–923, June 2016.
- <sup>11</sup>Sarah L Price and Jan Gerit Brandenburg. Molecular crystal structure prediction. In *Non-Covalent Interactions in Quantum Chemistry and Physics*, pages 333–363. Elsevier, 2017.
- <sup>12</sup>Angeles Pulido, Linjiang Chen, Tomasz Kaczorowski, Daniel Holden, Marc A. Little, Samantha Y. Chong, Benjamin J. Slater, David P. McMahon, Baltasar Bonillo, Chloe J. Stackhouse, Andrew Stephenson, Christopher M. Kane, Rob Clowes, Tom Hasell, Andrew I. Cooper, and Graeme M. Day. Functional materials discovery using energy–structure–function maps. *Nature*, 543(7647):657–664, March 2017.
- <sup>13</sup>Graeme M. Day and Andrew I. Cooper. Energy-structure-function maps: Cartography for materials discovery. *Advanced Materials*, 30(37):1704944, December 2017.
- <sup>14</sup>Anthony M Reilly, Richard I Cooper, Claire S Adjiman, Saswata Bhattacharya, A Daniel Boese, Jan Gerit Brandenburg, Peter J Bygrave, Rita Bylsma, Josh E Campbell, Roberto Car, et al. Report on the sixth blind test of organic crystal structure prediction methods. *Acta Crystallographica Section B: Structural Science, Crystal Engineering and Materials*, 72(4):439–459, 2016.
- <sup>15</sup>Noa Marom, Robert A DiStasio, Viktor Atalla, Sergey Levchenko, Anthony M Reilly, James R Chelikowsky, Leslie Leiserowitz, and Alexandre Tkatchenko. Many-body dispersion interactions in molecular crystal polymorphism. *Angew. Chem., Int. Ed.*, 52(26):6629–6632, 2013.
- <sup>16</sup>Johannes Hoja, Hsin-Yu Ko, Marcus A Neumann, Roberto Car, Robert A DiStasio, and Alexandre Tkatchenko. Reliable and practical computational description of molecular crystal polymorphs. *Science advances*, 5(1):eaau3338, 2019.
- <sup>17</sup>Dominik Fritz, Vagelis A Harmandaris, Kurt Kremer, and Nico FA van der Vegt. Coarse-grained polymer melts based on isolated atomistic chains: simulation of polystyrene of different tacticities. *Macromolecules*, 42(19):7579–7588, 2009.
- <sup>18</sup>C De Rosa, G Guerra, V Petraccone, and P Corradini. Crystal structure of the  $\alpha$ -form of syndiotactic polystyrene. *Polym. J.*, 23(12):1435, 1991.
- <sup>19</sup>Paolo Corradini, Claudio De Rosa, Gaetano Guerra, Roberto Napolitano, Vittorio Petraccone, and Beniamino Pirozzi. Conformational and packing energy of the crystalline  $\alpha$  modification of syndiotactic polystyrene. *Eur. Polym. J.*, 30(10):1173–1177, 1994.
- <sup>20</sup>Claudio De Rosa. Crystal structure of the trigonal modification ( $\alpha$  form) of syndiotactic polystyrene. *Macromolecules*, 29(26):8460–8465, 1996.
- <sup>21</sup>Laurent Cartier, Takumi Okihara, and Bernard Lotz. The  $\alpha$  “superstructure” of syndiotactic polystyrene: A frustrated structure. *Macromolecules*, 31(10):3303–3310, 1998.
- <sup>22</sup>C De Rosa, M Rapacciuolo, G Guerra, V Petraccone, and P Corradini. On the crystal structure of the orthorhombic form of syndiotactic polystyrene. *Polymer*, 33(7):1423–1428, 1992.
- <sup>23</sup>Yozo Chatani, Yukio Shimane, Toshikazu Ijitsu, and Toshimitsu Yukinari. Structural study on syndiotactic polystyrene: 3. crystal structure of planar form i. *Polymer*, 34(8):1625–1629, 1993.
- <sup>24</sup>Gaetano Guerra, Vincenzo M Vitagliano, Claudio De Rosa, Vittorio Petraccone, and Paolo Corradini. Polymorphism in melt crystallized syndiotactic polystyrene samples. *Macromolecules*, 23(5):1539–1544, 1990.
- <sup>25</sup>Ya Sen Sun and EM Woo. Relationships between polymorphic crystals and multiple melting peaks in crystalline syndiotactic polystyrene. *Macromolecules*, 32(23):7836–7844, 1999.
- <sup>26</sup>Eamom M Woo, Ya Sen Sun, and Meng Lu Lee. Crystal forms in cold-crystallized syndiotactic polystyrene. *Polymer*, 40(15):4425–4429, 1999.
- <sup>27</sup>RH Lin and EM Woo. Melting behavior and identification of polymorphic crystals in syndiotactic polystyrene. *Polymer*, 41(1):121–131, 2000.
- <sup>28</sup>Ya-Sen Sun and Eamom M Woo. Morphology and crystal structure of cold-crystallized syndiotactic polystyrene. *Polymer*, 42(5):2241–2245, 2001.
- <sup>29</sup>Yoshinori Tamai and Mitsuhiro Fukuda. Nanoscale molecular cavity in crystalline polymer membranes studied by molecular dynamics simulation. *Polymer*, 44(11):3279–3289, 2003.
- <sup>30</sup>Giuseppe Milano, Gaetano Guerra, and Florian Müller-Plathe. Anisotropic diffusion of small penetrants in the  $\delta$  crystalline phase of syndiotactic polystyrene: a molecular dynamics simulation study. *Chem. Mater.*, 14(7):2977–2982, 2002.
- <sup>31</sup>Yoshinori Tamai and Mitsuhiro Fukuda. Fast one-dimensional gas transport in molecular capillary embedded in polymer crystal. *Chem. Phys. Lett.*, 371(1-2):217–222, 2003.
- <sup>32</sup>Yoshinori Tamai and Mitsuhiro Fukuda. Reorientational dynamics of aromatic molecules clathrated in  $\delta$  form of crystalline syndiotactic polystyrene. *Chem. Phys. Lett.*, 371(5-6):620–625, 2003.
- <sup>33</sup>Yoshinori Tamai, Yoshiharu Tsujita, and Mitsuhiro Fukuda. Reorientational relaxation of aromatic molecules in the molecular cavity of crystalline syndiotactic polystyrene studied by molecular dynamics simulation. *J. Mol. Struct.*, 739(1-3):33–40, 2005.
- <sup>34</sup>Susana Figueroa-Gerstenmaier, Christophe Daniel, Giuseppe Milano, Gaetano Guerra, Olena Zavorotynska, Jenny G Vitillo, Adriano Zecchina, and Giuseppe Spoto. Storage of hydrogen as a guest of a nanoporous polymeric crystalline phase. *Phys. Chem. Chem. Phys.*, 12(20):5369–5374, 2010.
- <sup>35</sup>Susana Figueroa-Gerstenmaier, Christophe Daniel, Giuseppe Milano, Jenny G Vitillo, Olena Zavorotynska, Giuseppe Spoto, and Gaetano Guerra. Hydrogen adsorption by  $\delta$  and  $\epsilon$  crystalline phases of syndiotactic polystyrene aerogels. *Macromolecules*, 43(20):8594–8601, 2010.
- <sup>36</sup>Luigi Sanguigno, Francesco Cosentino, Domenico Larobina, and Giuseppe Mensitieri. Molecular simulation of carbon dioxide sorption in nanoporous crystalline phase of syndiotactic polystyrene. *Soft Mater.*, 9(2-3):169–182, 2011.
- <sup>37</sup>WG Noid. Perspective: Coarse-grained models for biomolecular systems. *The Journal of chemical physics*, 139(9):09B201\_1, 2013.
- <sup>38</sup>Chan Liu, Kurt Kremer, and Tristan Bereau. Polymorphism of syndiotactic polystyrene crystals from multiscale simulations. *Advanced Theory and Simulations*, 1(7):1800024, 2018.
- <sup>39</sup>Alessandro Laio and Francesco L Gervasio. Metadynamics: a method to simulate rare events and reconstruct the free energy in biophysics, chemistry and material science. *Reports on Progress in Physics*, 71(12):126601, 2008.
- <sup>40</sup>O. Valsson, P. Tiwary, and M. Parrinello. Enhancing important fluctuations: Rare events and metadynamics from a conceptual viewpoint. *Ann. Rev. Phys. Chem.*, 67(1):159–184, 2016.
- <sup>41</sup>Stefano Piana and Alessandro Laio. A bias-exchange approach to protein folding. *The journal of physical chemistry B*, 111(17):4553–4559, 2007.
- <sup>42</sup>Fabrizio Marinelli, Fabio Pietrucci, Alessandro Laio, and Stefano Piana. A kinetic model of trp-cage folding from multiple biased molecular dynamics simulations. *PLoS computational biology*, 5(8):e1000452, 2009.
- <sup>43</sup>Fahimeh Baftizadeh, Pilar Cossio, Fabio Pietrucci, and Alessandro Laio. Protein folding and ligand-enzyme binding from biased-exchange metadynamics simulations. *Current Physical Chemistry*, 2(1):79–91, 2012.
- <sup>44</sup>Jim Pfandtner and Massimiliano Bonomi. Efficient sampling of high-dimensional free-energy landscapes with parallel bias metadynamics. *Journal of Chemical Theory and Computation*, 11(11):5062–5067, October 2015.



- <sup>45</sup>Eamor M Woo, Ya-Sen Sun, and C-P Yang. Polymorphism, thermal behavior, and crystal stability in syndiotactic polystyrene vs. its miscible blends. *Progress in polymer science*, 26(6):945–983, 2001.
- <sup>46</sup>Federico Giberti, Matteo Salvalaglio, Marco Mazzotti, and Michele Parrinello. Insight into the nucleation of urea crystals from the melt. *Chemical Engineering Science*, 121:51–59, 2015.
- <sup>47</sup>Emiliano Brini, Valentina Marcon, and Nico FA van der Vegt. Conditional reversible work method for molecular coarse graining applications. *Phys. Chem. Chem. Phys.*, 13(22):10468–10474, 2011.
- <sup>48</sup>Gregor Deichmann and Nico FA van der Vegt. Conditional reversible work coarse-grained models of molecular liquids with coulomb electrostatics—a proof of concept study on weakly polar organic molecules. *J. Chem. Theory Comput.*, 13(12):6158–6166, 2017.
- <sup>49</sup>Francesco Luigi Gervasio, Alessandro Laio, and Michele Parrinello. Flexible docking in solution using metadynamics. *Journal of the American Chemical Society*, 127(8):2600–2607, 2005.
- <sup>50</sup>Giovanni Bussi, Francesco Luigi Gervasio, Alessandro Laio, and Michele Parrinello. Free-energy landscape for  $\beta$  hairpin folding from combined parallel tempering and metadynamics. *Journal of the American Chemical Society*, 128(41):13435–13441, 2006.
- <sup>51</sup>G Fiorin, A Pastore, P Carloni, and Michele Parrinello. Using metadynamics to understand the mechanism of calmodulin/target recognition at atomic detail. *Biophysical journal*, 91(8):2768–2777, 2006.
- <sup>52</sup>Federica Trudu, Davide Donadio, and Michele Parrinello. Freezing of a lennard-jones fluid: From nucleation to spinodal regime. *Physical review letters*, 97(10):105701, 2006.
- <sup>53</sup>D Quigley and PM Rodger. Metadynamics simulations of ice nucleation and growth. *The Journal of chemical physics*, 128(15):154518, 2008.
- <sup>54</sup>D Quigley and P Mark Rodger. Free energy and structure of calcium carbonate nanoparticles during early stages of crystallization, 2008.
- <sup>55</sup>Paul J Steinhardt, David R Nelson, and Marco Ronchetti. Icosahedral bond orientational order in supercooled liquids. *Physical Review Letters*, 47(18):1297, 1981.
- <sup>56</sup>Paul J Steinhardt, David R Nelson, and Marco Ronchetti. Bond-orientational order in liquids and glasses. *Physical Review B*, 28(2):784, 1983.
- <sup>57</sup>Min Jae Ko, Numan Waheed, Marc S Lavine, and Gregory C Rutledge. Characterization of polyethylene crystallization from an oriented melt by molecular dynamics simulation. *The Journal of chemical physics*, 121(6):2823–2832, 2004.
- <sup>58</sup>Numan Waheed, Min Jae Ko, and GC Rutledge. Molecular simulation of crystal growth in long alkanes. *Polymer*, 46(20):8689–8702, 2005.
- <sup>59</sup>Erik E Santiso and Bernhardt L Trout. A general set of order parameters for molecular crystals. *The Journal of chemical physics*, 134(6):064109, 2011.
- <sup>60</sup>Alessandro Barducci, Giovanni Bussi, and Michele Parrinello. Well-tempered metadynamics: a smoothly converging and tunable free-energy method. *Physical review letters*, 100(2):020603, 2008.
- <sup>61</sup>Alessandro Laio and Michele Parrinello. Escaping free-energy minima. *Proceedings of the National Academy of Sciences*, 99(20):12562–12566, 2002.
- <sup>62</sup>Alessandro Barducci, Massimiliano Bonomi, and Michele Parrinello. Metadynamics. *Wiley Interdisciplinary Reviews: Computational Molecular Science*, 1(5):826–843, 2011.
- <sup>63</sup>Cameron Abrams and Giovanni Bussi. Enhanced sampling in molecular dynamics using metadynamics, replica-exchange, and temperature-acceleration. *Entropy*, 16(1):163–199, 2014.
- <sup>64</sup>James F Dama, Michele Parrinello, and Gregory A Voth. Well-tempered metadynamics converges asymptotically. *Physical review letters*, 112(24):240602, 2014.
- <sup>65</sup>Pratyush Tiwary and Michele Parrinello. A time-independent free energy estimator for metadynamics. *The Journal of Physical Chemistry B*, 119(3):736–742, 2014.
- <sup>66</sup>Paolo Raiteri, Alessandro Laio, Francesco Luigi Gervasio, Cristian Micheletti, and Michele Parrinello. Efficient reconstruction of complex free energy landscapes by multiple walkers metadynamics. *The journal of physical chemistry B*, 110(8):3533–3539, 2006.
- <sup>67</sup>Mark James Abraham, Teemu Murtola, Roland Schulz, Szilárd Páll, Jeremy C Smith, Berk Hess, and Erik Lindahl. Gromacs: High performance molecular simulations through multi-level parallelism from laptops to supercomputers. *SoftwareX*, 1:19–25, 2015.
- <sup>68</sup>Gareth A Tribello, Massimiliano Bonomi, Davide Branduardi, Carlo Camilloni, and Giovanni Bussi. Plumed 2: New feathers for an old bird. *Computer Physics Communications*, 185(2):604–613, 2014.
- <sup>69</sup>The PLUMED Consortium. Promoting transparency and reproducibility in enhanced molecular simulations. *Nat. Methods*, 16:670–673, 2019. For the full list of researches from the PLUMED Consortium, see <https://www.plumed-nest.org/consortium.html>.
- <sup>70</sup>Giovanni Bussi, Davide Donadio, and Michele Parrinello. Canonical sampling through velocity rescaling. *J. Chem. Phys.*, 126(1):014101, 2007.
- <sup>71</sup>Michele Parrinello and Aneesur Rahman. Polymorphic transitions in single crystals: A new molecular dynamics method. *Journal of Applied physics*, 52(12):7182–7190, 1981.
- <sup>72</sup>Kieron Burke. Perspective on density functional theory. *J. Chem. Phys.*, 136:150901, 2012.
- <sup>73</sup>Axel D. Becke. Perspective: Fifty years of density-functional theory in chemical physics. *J. Chem. Phys.*, 140:18A301, 2014.
- <sup>74</sup>Haoyu S Yu, Shaohong L Li, and Donald G Truhlar. Perspective: Kohn-sham density functional theory descending a staircase. *J. Chem. Phys.*, 145:130901, 2016.
- <sup>75</sup>R. J. Maurer, C. Freysoldt, A. M. Reilly, J. G. Brandenburg, O. T. Hofmann, T. Björkman, S. Lebègue, and A. Tkatchenko. Advances in density-functional calculations for materials modeling. *Annu. Rev. Mater. Res.*, 49:3.1–3.30, 2019.
- <sup>76</sup>J. G. Brandenburg, E. Caldeweyher, and S. Grimme. Screened exchange hybrid density functional for accurate and efficient structures and interaction energies. *Phys. Chem. Chem. Phys.*, 18:15519–15523, 2016.
- <sup>77</sup>E. Caldeweyher and J. G. Brandenburg. Simplified dft methods for consistent structures and energies of large systems. *J. Phys.: Condens. Matter*, 30:213001, 2018.
- <sup>78</sup>R. Sure and S. Grimme. *Chem. Eur. J.*, 23:5687–5691, 2017.
- <sup>79</sup>S. Roesel, H. Quanz, C. Logemann, J. Becker, E. Mossou, L. C. Delgado, E. Caldeweyher, S. Grimme, and P. R. Schreiner. London dispersion enables the shortest intermolecular hydrocarbon h...h contact. *J. Am. Chem. Soc.*, 139:428–7431, 2017.
- <sup>80</sup>S. Grimme, A. Hansen, J. G. Brandenburg, and C. Bannwarth. Dispersion-corrected mean-field electronic structure methods. *Chem. Rev.*, 116:5105–5154, 2016.
- <sup>81</sup>Gregory J. O. Beran. Modeling polymorphic molecular crystals with electronic structure theory. *Chem. Rev.*, 116(9):5567–5613, 2016.
- <sup>82</sup>J. Klimeš and A. Michaelides. Perspective: Advances and challenges in treating van der waals dispersion forces in density functional theory. *J. Chem. Phys.*, 137:120901, 2012.
- <sup>83</sup>A. Erba, J. Baima, I. Bush, R. Orlando, and R. Dovesi. Large-scale condensed matter dft simulations: Performance and capabilities of the crystal code. *J. Chem. Theory Comput.*, 13:5019–5027, 2017.
- <sup>84</sup>Roberto Dovesi, Alessandro Erba, Roberto Orlando, Claudio M. Zicovich-Wilson, Bartolomeo Civalleri, Lorenzo Maschio, Michel Rérat, Silvia Casassa, Jacopo Baima, Simone Salustro, and Bernard Kirtman. *WIREs Comput. Mol. Sci.*, 8:e1360, 2018.
- <sup>85</sup>R. Sure and S. Grimme. Corrected small basis set hartree-fock method for large systems. *J. Comput. Chem.*, 34:1672–1685, 2013.

- <sup>86</sup>M. Cutini, B. Civalleri, M. Corno, R. Orlando, J. G. Brandenburg, L. Maschio, and P. Uglieri. Assessment of different quantum mechanical methods for the prediction of structure and cohesive energy of molecular crystals. *J. Chem. Theory Comput.*, 12:3340–3352, 2016.
- <sup>87</sup>M. Elstner, D. Porezag, G. Jungnickel, J. Elsner, M. Haugk, T. Frauenheim, S. Suhai, and G. Seifert. Self-consistent-charge density-functional tight-binding method for simulations of complex materials properties. *Phys. Rev. B*, 58(11):7260–7268, 1998.
- <sup>88</sup>B. Aradi, B. Hourahine, and Th. Frauenheim. Dftb+, a sparse matrix-based implementation of the dftb method. *J. Phys. Chem. A*, 111(26):5678–5684, 2007.
- <sup>89</sup>J. G. Brandenburg and S. Grimme. Accurate Modeling of Organic Molecular Crystals by Dispersion-Corrected Density Functional Tight Binding (DFTB). *J. Phys. Chem. Lett.*, 5:1785–1789, 2014.
- <sup>90</sup>J. G. Brandenburg, J. Potticary, H. A. Sparkes, S. L. Price, and S. R. Hall. Thermal expansion of carbamazepine: Systematic crystallographic measurements challenge quantum chemical calculations. *J. Phys. Chem. Lett.*, 8:4319–4324, 2017.